Supplementary Information

Direct 3D print polyimide aerogels for synergy management of thermal insulation, gas permeability and light absorption

Jianming Yang[‡], Jialu Lu[‡], Shuang Xi, Hongqiang Wang, Dongxiao Han, Caide Fan, Zhihua Zhang, Jun Shen, Bin Zhou*, and Ai Du*

Shanghai Key Laboratory of Special Artificial Microstructure Materials and Technology, School of Physics Science and Engineering, Tongji University, Shanghai 200092, China

*E-mail: zhoubin863@tongji.edu.cn (*Prof.* B. Zhou); duai@tongji.edu.cn (*Prof.* A. Du)

Keywords: 3D printing, polyimide aerogels, chemical imidization, thermal insulation, gas permeability, light absorption

Table of Contents

1. Experimental Section

Materials: 2,2'-dimethyl-[1,1'-biphenyl]-4,4'-diamine (DMBZ, ≥99.0%), and benzophenone-3,3',4,4'-tetracarboxylic dianhydride (BTDA, 99.0%) were purchased from Macklin Biochemical Co., Ltd. (Shanghai, China). 1,3,5-tris(4-aminophenoxy) benzene (TAB, 97.0%), 1-methyl-2-pyrrolidone (NMP, ≥99.0%), acetic anhydride (AA, ≥98.5%), pyridine (PD, ≥99.5%), carbon nanotubes (CNTs, carboxylic multi-walled, >95%, inner diameter: 3-5 nm, outer diameter: 8−15 nm, length: 0.5−2 μm), aqueous ammonia (25.0−28.0 %) and ethanol absolute (≥99.7%) were purchased from Sinopharm Chemical Reagent Co., Ltd. (Beijing, China). All of reagents were used directly without further purification.

Preparation of PA inks: The PA inks were prepared by mixing DMBZ with BTDA in NMP with a molar ratio of 1: 1. Specifically, first, the precursor solution was obtained by sequentially dispersing 1.815 g (8.55 mmol) DMBZ and 2.754 g (8.55 mmol) BTDA in 40 mL NMP. Next, 0.034 g (0.09 mmol) of TAB was added to the precursor solution as a cross-linking agent, and after sufficiently stirring for 40 min, the corresponding dehydrating agent (a mixed solvent of AA and PD, with the molar ratio of AA: PD: BTDA kept at m: m: 1, where m was 6, 5, 4, 3, 2, and 1, respectively) was added. The above mixed solutions were vigorously stirred for 10 min, and then naturally incubated about 1.2, 1.8, 2.9, 6.0, 36, and 36 h (corresponding to m=6, 5, 4, 3, 2, and 1, respectively), respectively, the polyimide aerogel-based sol-gel inks (PA inks for short) were obtained. The resultant PA inks were referred to as PA-A, PA-B, PA-C, PA-D, PA-E, and PA-F, respectively. Note that, all preparation processes of PA inks were carried out at room temperature (~25 °C), and PA-F did not gel.

Preparation of PA/CNT inks: The PA/CNT inks were prepared by using the above-mentioned PA-D as a matrix. The preparation procedure was exactly the same as the preparation of PA-D, except that before adding the dehydrating reagent, CNTs (mass fraction: 5.5, 11 and 16.4 wt%, relative to polyamide acid precursors: DMBZ and BTDA) were fully dispersed into the precursor solution. The resultant PA inks were referred to as PA/CNT-5.5%, PA/CNT-11% and PA/CNT-16.4% respectively. For a convenient comparison, the PA-D without CNTs was also referred to as PA/CNT-0%.

Ink Rheological Measurements: The rheology of inks was characterized by using a rotational rheometer (HAAKE MARS 40, Thermo Scientific, Germany). The gelation processes of inks were monitored by up to 8 h of rheological tests with a cup measuring geometry (CC25 DIN/Ti-02190239, 5.3 mm gap) at a constant frequency of 1 Hz and a constant shear stress of 1 Pa, through an oscillatory logarithmic stress sweep mode. And a sample hood (POM) with integrated solvent trap was used to minimize solvent volatilization during rheological tests. The apparent viscosities were measured by using a parallel plate geometry (P20/Ti-02190120, 1 mm gap) with a shear rate ranging from 10^{-3} to 10^3 s^{-1} for 100 s, in a shear rate sweep mode. The storage (G′) and loss (G″) moduli were measured as a function of the shear stress ranging from 10^{-3} to $4{\times}10^3$ Pa at a constant frequency of 1 Hz, through an oscillatory logarithmic stress sweep mode. For all rheological tests, the temperature was set at 25 °C and controlled by Peltier.

3D Printing: 3D printing of polyimide aerogels (PAs) was performed under atmospheric conditions using a custom direct ink writing (DIW) 3D printer.[S1] The needle to connect the syringe was a tapered needle with an inner diameter of 410 μm. Applied pressure varied from the range of 10−85 psi (≈0.69−≈5.86 bar), and the translation speed of the needle was a constant value of 20 mm s^{-1}. As a display, the 3D structures with various shapes and sizes, including wafers (diameter: 30 mm), rectangles (horizontal dimension: 30×14 mm^2), squares (horizontal dimension: 20×20 mm^2, and 30×30 mm^2), cylinders (diameter: 30 mm), pyramids (horizontal dimension: 30×30 mm^2), and towers (horizontal dimension: 40×40 mm^2, and 20×20 mm^2) were printed. The printed structures were transferred to a container containing absolute ethanol to prevent shrinkage. After four times of solvent replacement (absolute ethanol, 12 h each time) and carbon dioxide supercritical drying, 3D-printed PAs were obtained and labeled according to the inks used. Note that, the labels (PA/CNT-0%, PA/CNT-5.5%, and PA/CNT-11%) all originated from the same package ratio of 90%, when comparing the attributes/or properties of 3D-printed PAs. For comparison, another packing ratio of 70% for 3D-printed PAs was also used, labeled PA-70%.

Characterizations: Microstructure images of 3D-printed PAs were observed on a scanning electron microscopy (SEM, ZEISS MERLIN Compact, Germany) with an EDS detector. Prior to the SEM observation, all printed samples (both in direct block and sliced form) and CNTs (in powder form) were tightly adhered to the sample stage with conductive tape, and subsequently sprayed with platinum for 120 s. The fiber width of 3D-printed PAs was statistically measured with a total of

100 counts via ImageJ. Fourier Transform Infrared (FTIR) spectra were obtained using a FTIR spectrometer (Thermo Scientific Nicolet iS5). Specifically, the samples were finely pulverized, and thoroughly ground yet mixed with potassium bromide with a mass ratio of 1:50, and then pressed into pieces for inspection. Nitrogen adsorption/desorption isotherms were measured by using Quantachrome autosorb iQ instrument (Micromeritics APSP 2460, America) after degassing at 120 °C for 12 h. The pore size distributions were obtained from the isotherms using the Barrett-Joyner-Halenda (BJH) model, specific surface areas were estimated by the Brunaur-Emmett-Teller (BET) method. The shrinkage was calculated by comparing the dimensional reduction ratios of the samples before and after drying. Thermal conductivity was measured by a heat conduction analyzer (Hot Disk TPS 2500S) under room temperature. The density was determined by the ratio of weight to volume. The measurements of shrinkage, thermal conductivity and density were the average of three tests. The hyperhydrophilicity and rapid water absorption of samples were tested by a contact angle/surface tension tester (Dataphysics DCAT21, Germany). Three-point bending tests were performed using a universal mechanical testing machine (INSTRON 5982, America) with the loading rate of 0.2 mm min^{-1} until the sample broke. The compressive stress-strain curves were obtained using a universal testing machine (AGS-X, Shimadzu Corporation, Japan) with a crosshead velocity of 0.2 mm min^{-1} until the strain reached 60%. The elastic modulus was calculated from the slope of the first 1−5% line segment of the compressive stress-strain curve.

Thermogravimetric analysis (TGA) was conducted on a thermogravimetric analyzer (TA SDT Q600, Mettler Toledo TGA/DSC 3^{+}, Netzsch Sta 409 PC) from 30 to 1000 °C under an air atmosphere at a heating rate of 10 °C min^{-1}. Thermal stability performance of 3D-printed PAs was directly assessed through a constant heated platform (X1010G, China) with gradual setting temperature of 50, 100, 170, 200, 300, 400, and 450 °C. Four samples were placed in parallel on the heated platform. To make all samples heated evenly, as well as the beauty of thermal images, a piece of glass was embedded between the samples and the heated platform. An infrared thermal imager (FOTRIC 220s, China) was simultaneously used to capture infrared images and temperature change of the sample surface and platform (the glass) with a detection distance of 0.6 m.

Air permeability of the samples was examined by a straightforward experiment setup inspired by the air permeability tests of concrete.[S2] Real-time monitoring of the air pressure inside the setup was undertaken using a digital differential pressure gauge (SUMMIT 655, Republic of Korea). The

outlet of a syringe was connected to a needle (22 G), which was then firmly inserted into the samples (all samples were pre-drilled with a hole slightly smaller than the outer diameter of the needle used). A precise dispenser pumped compressed air throughout the setup at a pressure of 5 psi (≈0.34 bar). The inlet pipe was clamped once the digital differential pressure gauge stabilized, and the measurements were continuously recorded until achieving a stable value. The ammonia adsorption capacity of the samples was also explored by real-time monitoring ammonia concentration in a confined space containing trace amounts of aqueous ammonia (Fig. S22, Supporting Information). To create a tight seal at the connection, the probe of an ammonia concentration detector (AR8500) was attached to a foam box using commercial insulating tapes. First, a beaker containing 10 µL of aqueous ammonia was swiftly loaded into a foam box, the cap was retained closed and maintained for 2 min (the detector has reached its maximum detection value of 100 ppm). Then, the cap was opened and the beaker was removed. The sample was swiftly added and the cap was swiftly closed, as soon as the detector concentration started to decline. The measurements were recorded in real time until achieving a stable value. After each test, the sample was placed in a special ventilation kitchen to remove the adsorbed ammonia, and then the measurement was repeated until 3 measurements were completed.

The reflectance and transmittance spectra of 3D-printed PAs were directly measured by using a UV-vis-NIR spectrophotometer (Jasco V-570, Japan) with an integrating sphere. The wavelength range was from 400 to 2000 nm. And the absorbance of the samples was calculated by removing the transmitted and reflected portions. A xenon lamp (HSX-F300, China) with a spectral range of 300 to 2500 nm and an AM1.5 filter provided the simulated sunlight. The sample was placed flat on a light-absorbing foam and kept perpendicular to sunlight. An infrared thermal imager (FOTRIC 220s, China) was used to capture infrared images and temperature changes of 3D-printed PAs from an initial state to an equilibrium state under one-sun irradiation with a detection distance of 0.6 m.

Thermal and/or Humidity Regulation Experiments: Thermal and/or humidity regulation experiments were carried out through a well-designed plastic foam box with effective sealing, as shown in Fig. S26, Supporting Information. The plastic foam box (inside diameter: 230×120×145 mm^3, external diameter: 274×164×181 mm^3) was finely designed into two chambers (C1, C2), the middle foam partition left a sample hole (30×30 mm^2, the sample used was a cylinder with a diameter of 30 mm, a height of ~18 mm and a package ratio of 90%), and some necessary insulation

tapes (polyimide film) ensured independence and effective sealing between C1 and C2, as well as the sealed insulation of the gaps between sample and sample hole. A temperature/humidity sensor (the measuring range is -40−80 °C/0−99.9 %RH) was placed in each chamber for real-time monitoring of temperature and humidity. The temperature and humidity conditions in the natural environment were simulated with hot water (~60 °C), ice (ice pack), and their combination. The temperature and humidity for each chamber were recorded in real time for 10 min, after that, the aforementioned conditions commenced for another 10 min. During testing, one count was collected per second, and when processing data, one data point was captured every 30 counts. Thermal and/or humidity regulation stability was measured by up to 6 h of testing with a hot water and ice combination, where hot water was updated every 30 min, and when processing data, one data point was captured every 500 counts. A combination of liquid nitrogen and hot water was also used to observe the thermal and/or humidity regulation capacity of the sample in an extreme environment.

Solar Steam Generation and Solar Seawater Purification Experiments: The solar steam generation and solar seawater purification experiments were conducted based on an early experimental setup of our group.[S1, S3] Succinctly, a xenon lamp (HSX-F300, China) with a spectral range of 300 to 2500 nm and an AM1.5 filter provided the simulated sunlight, an infrared thermal imager (FOTRIC 220s, China) was used to capture infrared images and temperature change curves of evaporators and water, and an electronic balance (BS124S, 0.0001 g, Germany) was used to measure the mass changes of water during the solar steam generation experiments of 1 h under one-sun illumination or at dark. Note that when performing the solar seawater purification experiment, an additional optically transparent glass mask was used to collect the vapors generated on the sample surface. The concentrations of metal ions (Na^+, Mg^{2+}, K^+, Ca^{2+}) in sea water and steam water were measured using an inductively coupled plasma emission spectrometer (ICP-OES/MS). The evaporation rate was obtained by linear fitting in the steady-state region of the curve representing the change in mass of water. And the efficiency (η) was calculated as follows:

$$\eta = \frac{\dot{m}h_{LV}}{C_{opt}I} \tag{S-1}$$

where $\dot{m}$ is the difference of mass flux (with and without light, kg m^{-2} h^{-1}), C_{opt} (=1) represents the optical concentration, I is the normal direct solar illumination (1 kW m^{-2} for one sun). h_{LV} denotes the liquid–vapor phase change enthalpy (including sensible heat and phase-change enthalpy, J kg^{-1}), which is calculated by:

$$h_{LV} = C\Delta T + \Delta H_{vap} \qquad\qquad (\text{S-2})$$

where C is the specific heat capacity of water (4.18 kJ kg^{-1} K^{-1}), ΔT is the temperature difference (K) between the evaporator surface and ambient condition. ΔH_{vap} is the latent heat of phase change, which can be considered as 2256 kJ kg^{-1}.[S4]
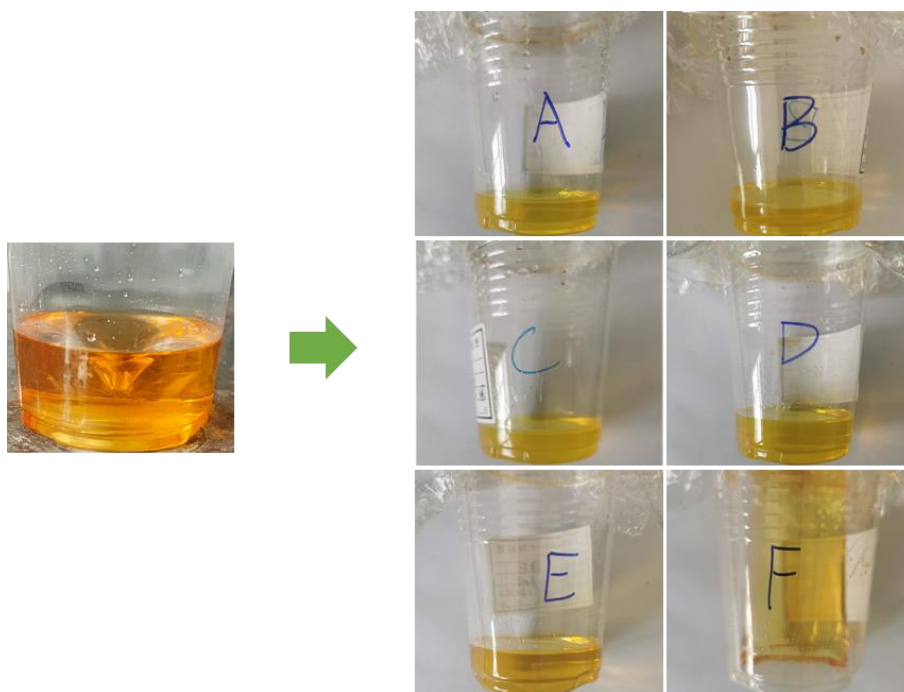
2. Supplementary Figures

Fig. S1. The photos of PA inks: Stirring of polyamic acid solution (left) and aging of PA inks for 60 days (right). Note that, PA-(A-E) can gel, PA-F cannot gel.
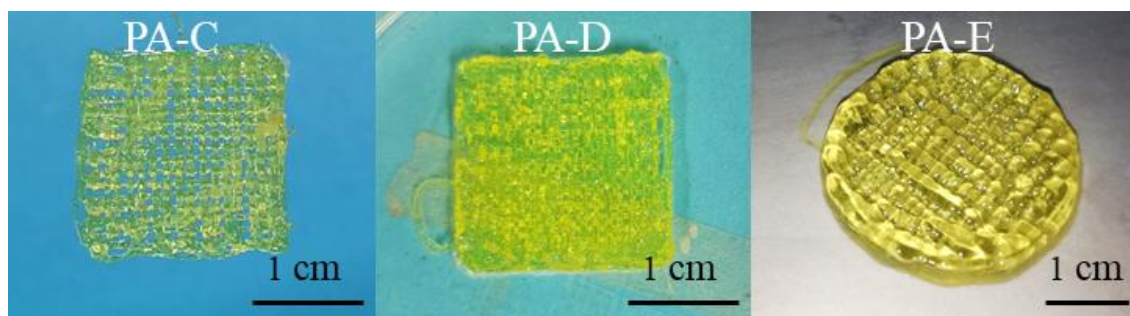
Fig. S2. The photos of 3D-printed structures by using the three PA inks: PA-C, PA-D, and PA-E.
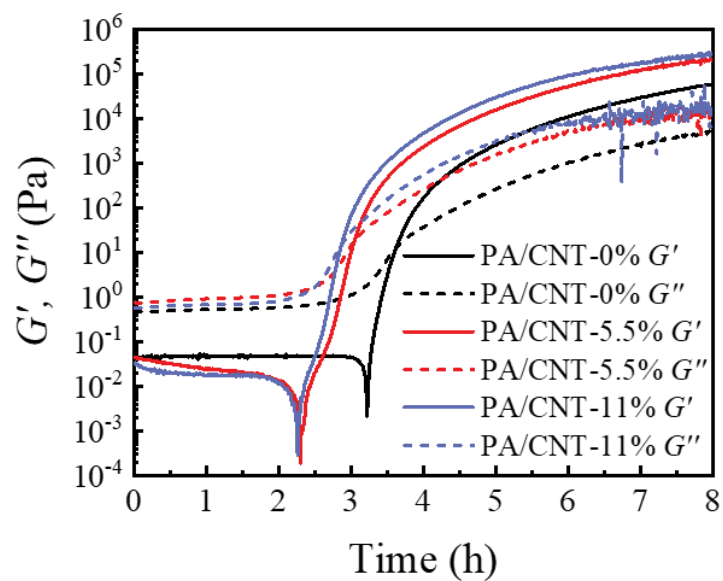
Fig. S3. The on-going evolution of storage (G') and loss (G'') moduli for PA/CNT-0%, PA/CNT-5.5%, and PA/CNT-11% inks over time.
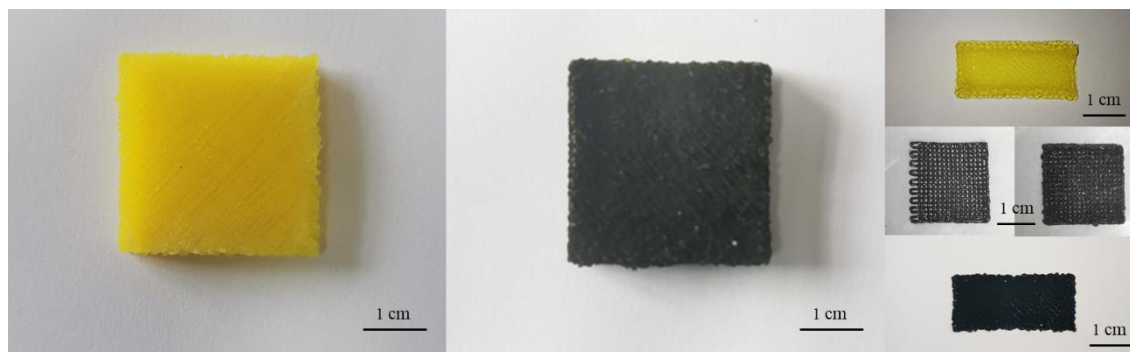
Fig. S4. The photographs of 3D-printed PA/CNT-0% (yellow) and PA/CNT-11% (black).

Fig. S5. The photographs of the plastic cup's bottom (red marked)-remaining PA ink with a higher CNT content of 16.4 wt%: a) the freshly prepared ink, b) the ink after resting for some time (before gelation); and c) a photograph of the needle (inner diameter: 410 μm) becoming blocked (red marked) when the ink (CNT content: 16.4 wt%) was forced out even at a maximum applied pressure of 85 psi (≈5.86 bar).
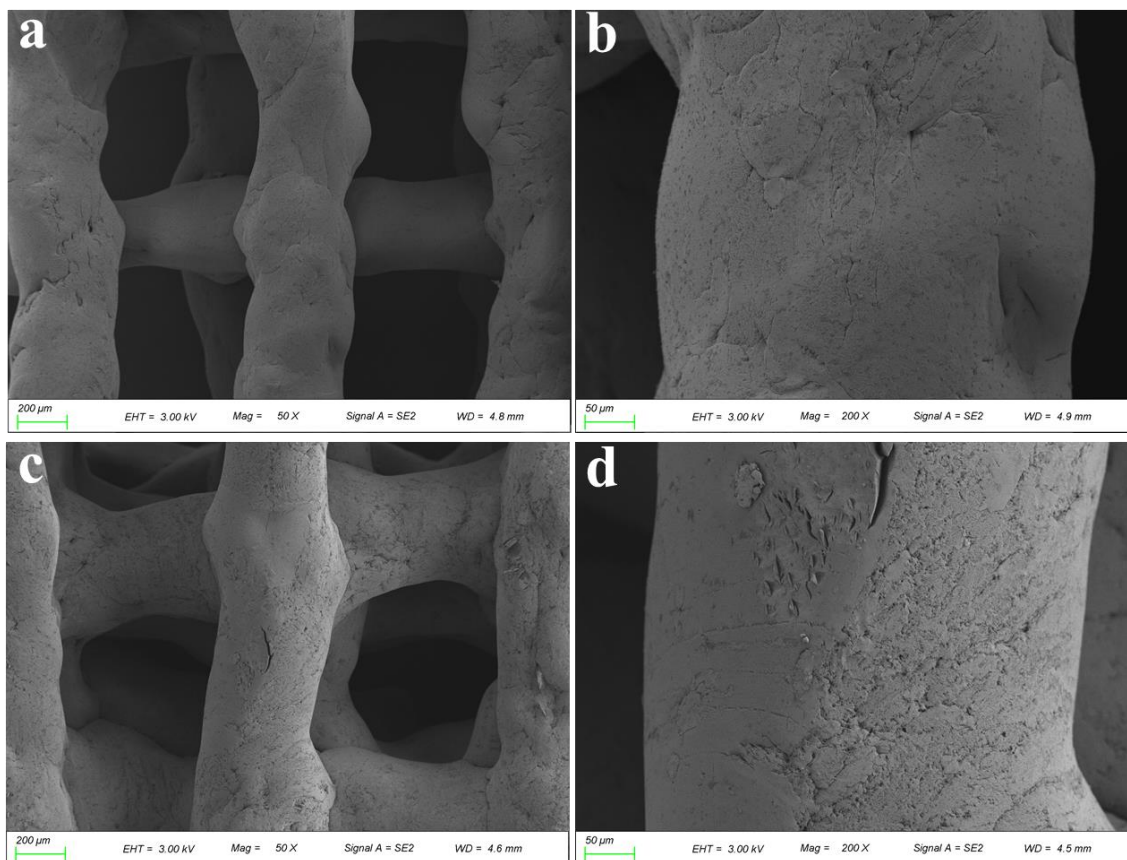
Fig. S6. The SEM images of the 3D-printed representative lattice-shaped PAs: a, b) PA/CNT-0%, and c, d) PA/CNT-11%.
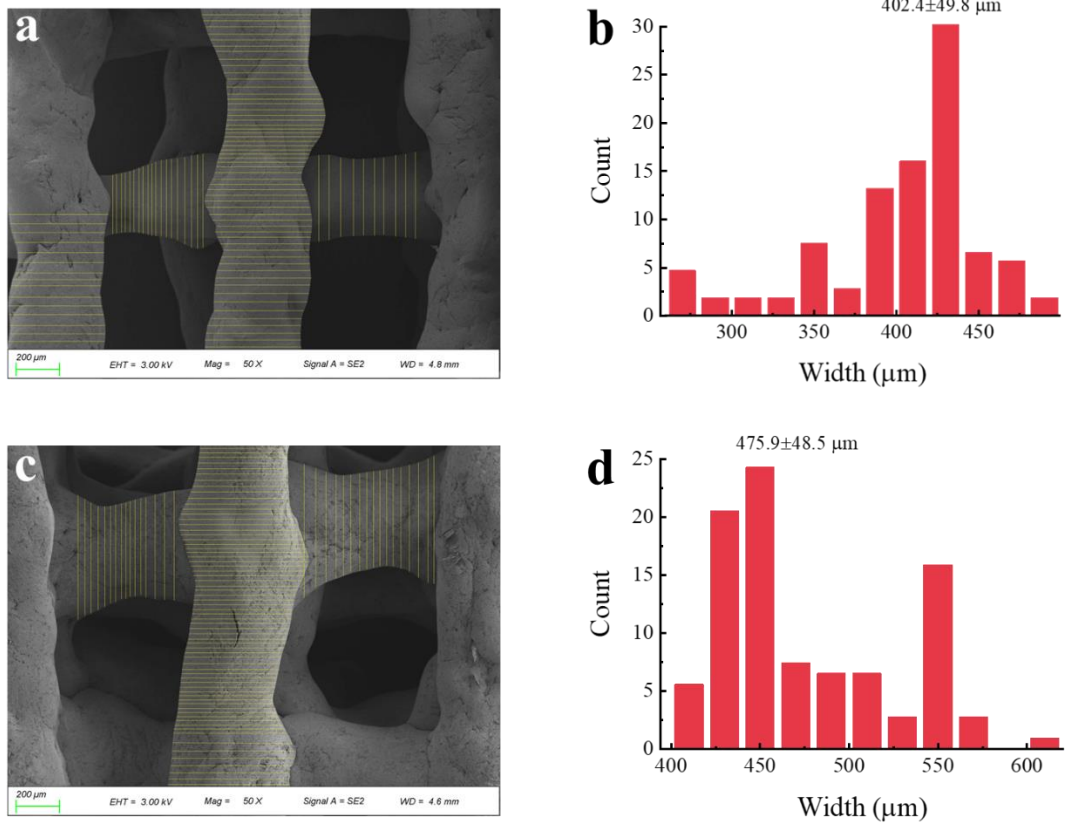
Fig. S7. The measuring trajectories of fiber width at 100 positions and the statistical distribution graphs of fiber width: a, b) PA/CNT-0%, and c, d) PA/CNT-11%.
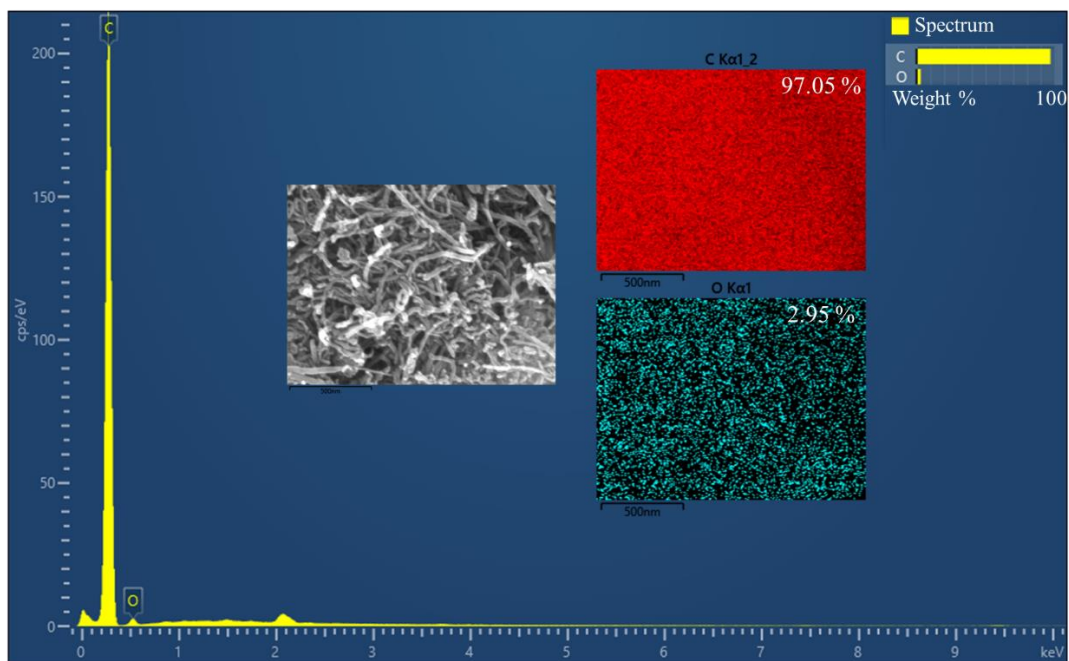
Fig. S8. The SEM-EDS mapping of CNTs.
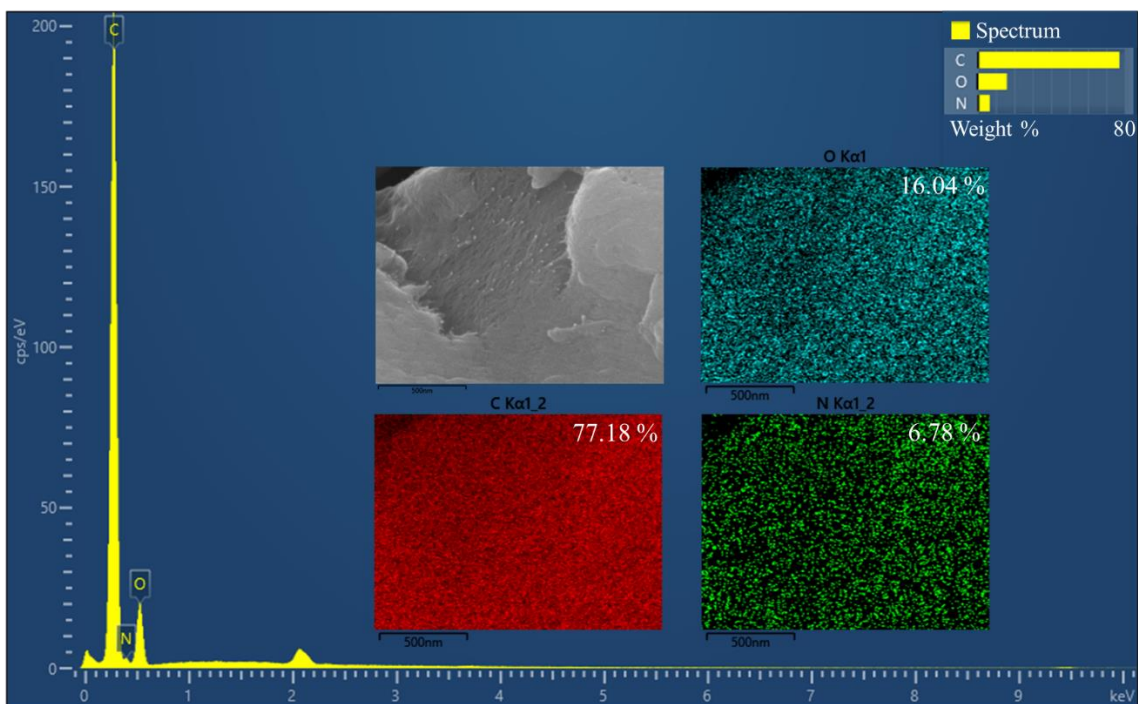
Fig. S9. The SEM-EDS mapping of PA/CNT-0%.
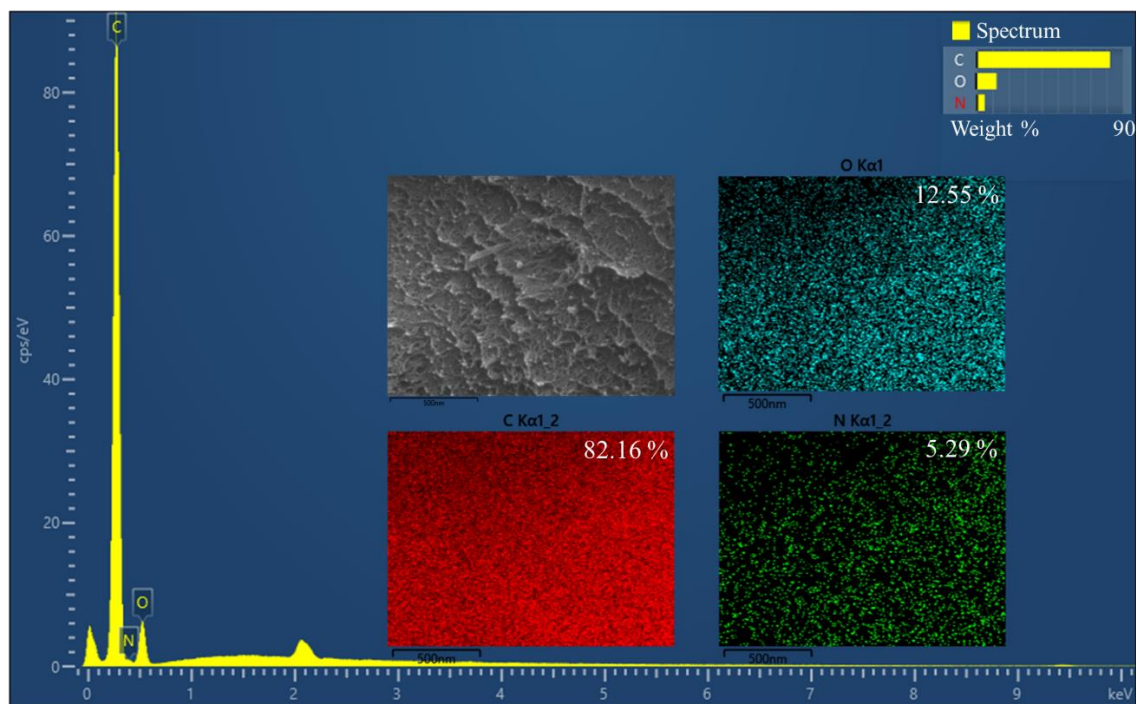
Fig. S10. The SEM-EDS mapping of PA/CNT-5.5%.
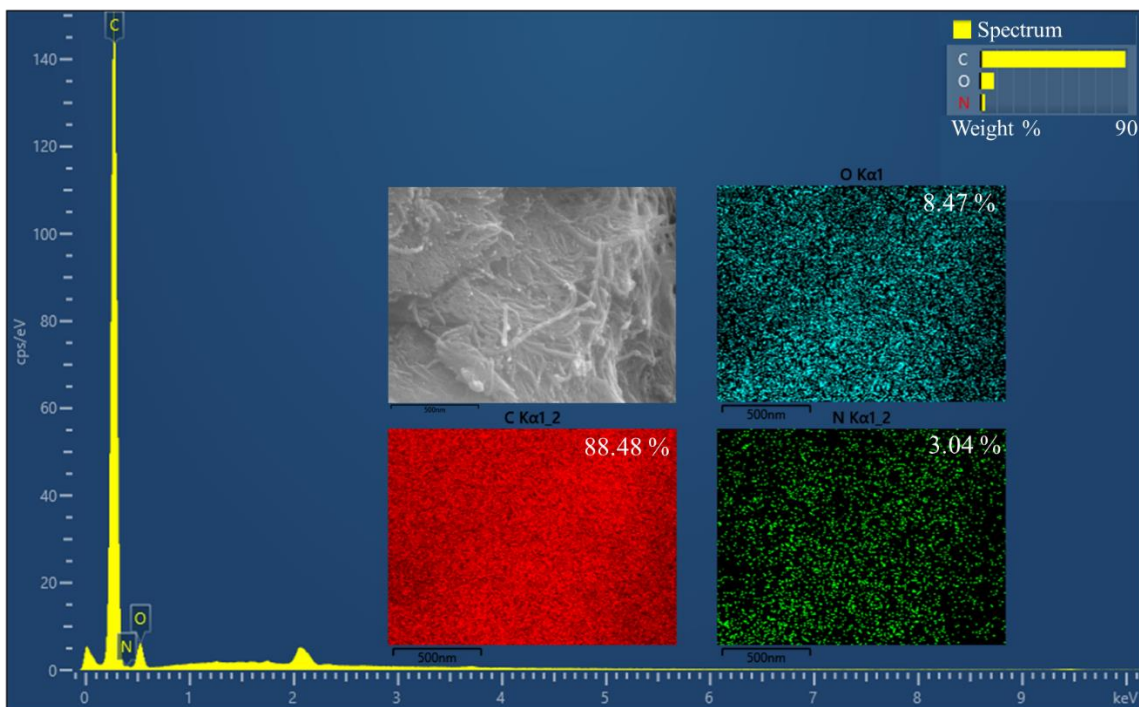
Fig. S11. The SEM-EDS mapping of PA/CNT-11%.
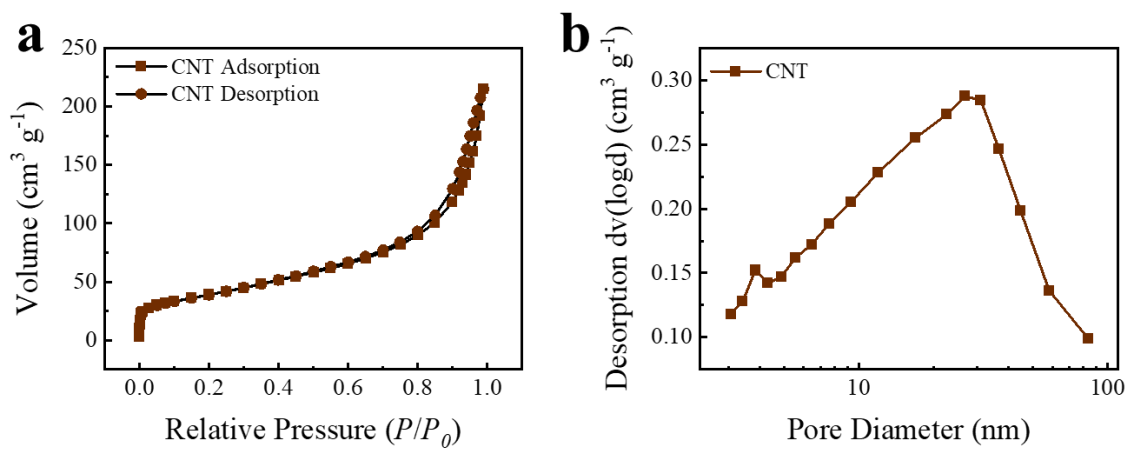
Fig. S12. The isotherm: a) and the pore-size distribution: b) of CNT.
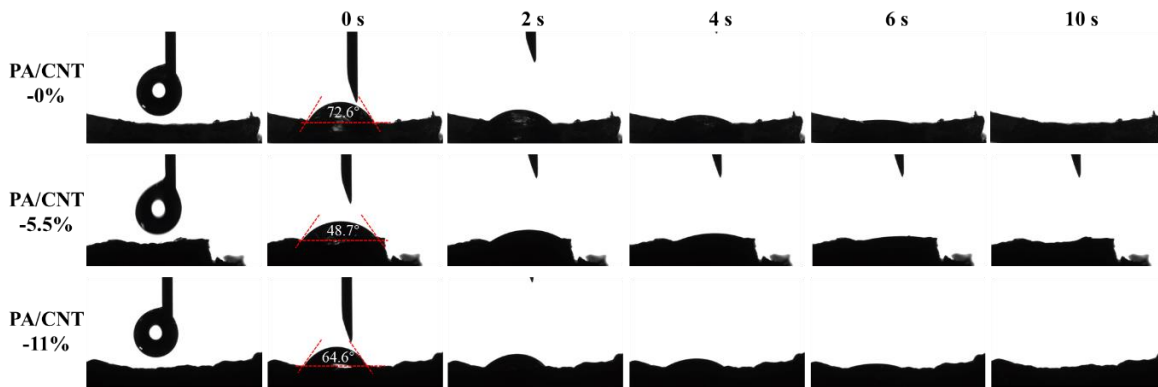
Fig. S13. The water droplet dynamic contact angle images of 3D-printed PAs. The aggregation of CNTs in 3D-printed PAs maybe alter the initial contact angles, and all 3D-printed PAs exhibited hyperhydrophilicity and quick water absorption (within 10 s).
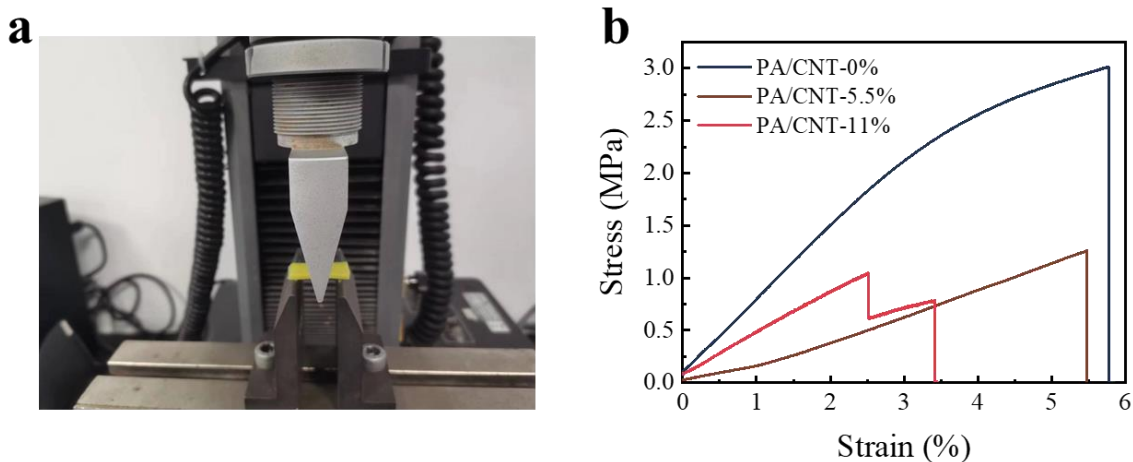
Fig. S14. The three-point bending tests of 3D-printed PAs: a) The photograph of the experiment. b) The stress−strain curves. The rectangular samples with the dimension of $30\times10\times2$ mm^3 were prepared for three-point bending tests. Note that the appearance of two segments of the sample PA/CNT-11% curve may be the incomplete fracture during the flexural test.
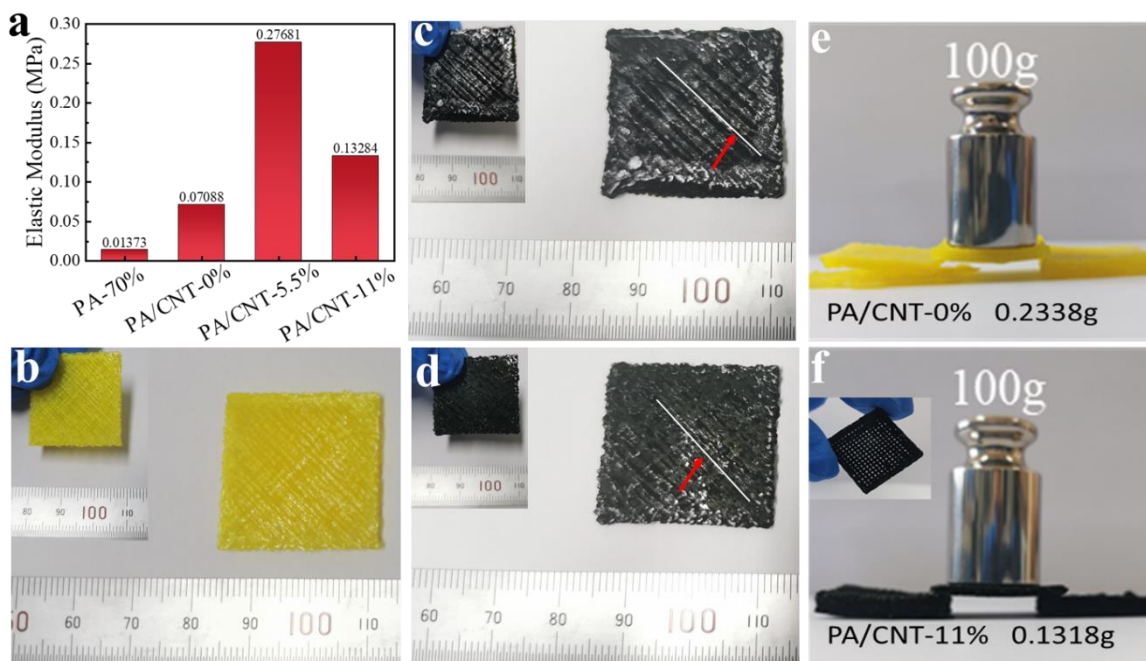
Fig. S15. The compressive tests of 3D-printed PAs: a) The elastic modulus. Note that, the elastic modulus of PA/CNT-11% is abnormally lower than that of PA/CNT-5.5%, possibly as a result of the sporadic cracks derived from uneven 3D-printed surfaces during tests. The photographs of 3D-printed PAs after compression tests: b) PA/CNT-0%; c) PA/CNT-5.5% and d) PA/CNT-11%. The photographs of printed aerogel sheets with a thickness of ~3.5 mm e), or even ~1.8 mm f) supporting a 100-g weight.

The location denoted by the red arrow (where the white line was drawn) showed that cracks (PA/CNT-0%, without cracks) had emerged after tests for PA/CNT-5.5% and PA/CNT-11%. This is because the flaky 3D-printed aerogel surface is uneven since they somewhat deformed throughout the drying process, as well as the samples became comparatively brittle after the addition of CNTs, which is consistent with the result of three-point bending tests. It is worth noting that the sample size (especially the small thickness: ~5 mm) may be unsuitable for compression tests. However, most aerogels can easily be crushed into powders or paper-thin monoliths due to their inherent brittleness or porosity, and here for the compression test results of 3D-printed PAs, their excellent mechanical properties can still be traced.
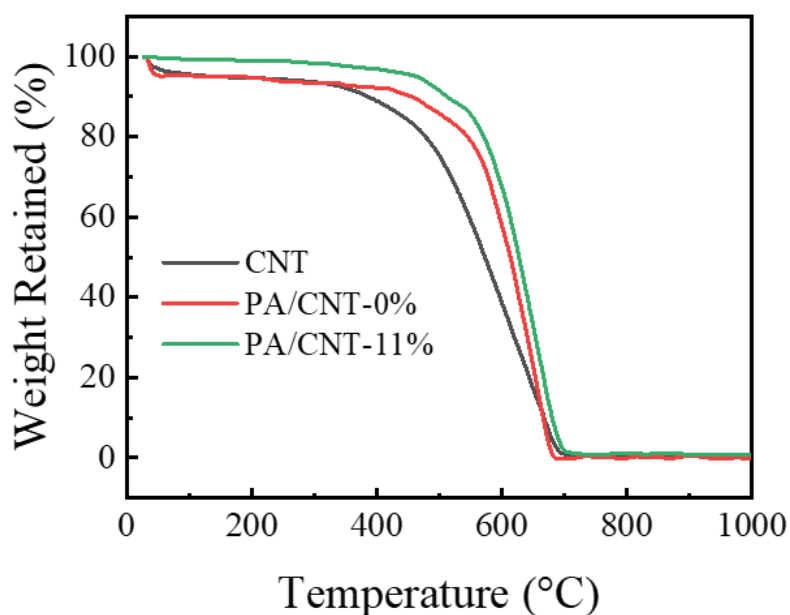
Fig. S16. The TGA curves of the representative 3D-printed PAs. The significant drop in curves during the initial heating phase was due to the inevitable water absorption of the samples in preservation. Therefore, this portion was deleted while determining the value of T_5.
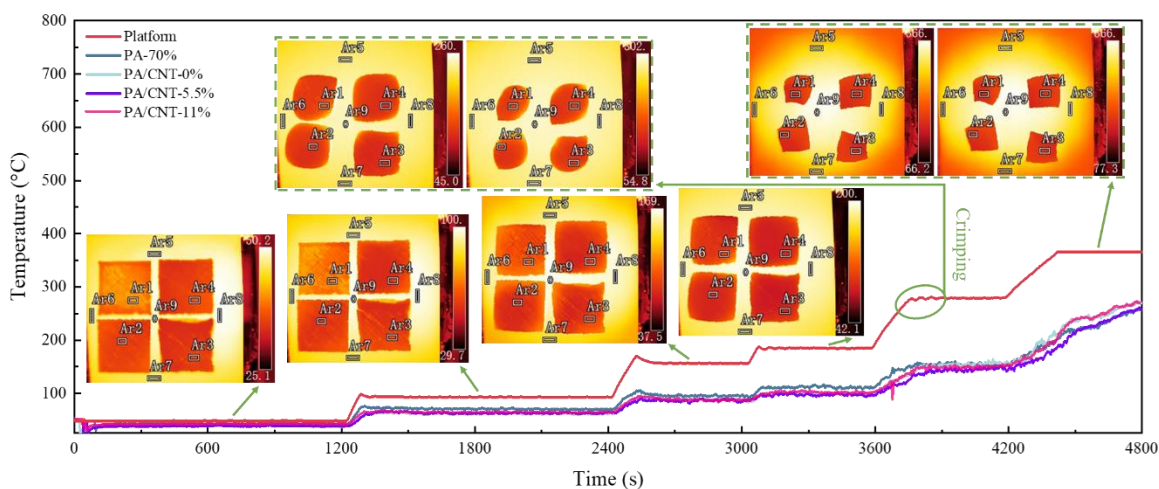

Fig. S17. The assessment of thermal insulation and stability of 3D-printed PAs. Note that, the temperature of the heated platform (the temperature curve of platform) cannot be accurately detected when the temperature surpasses 350 °C, since the short detection interval (0−350 °C) of the thermal imager utilized.
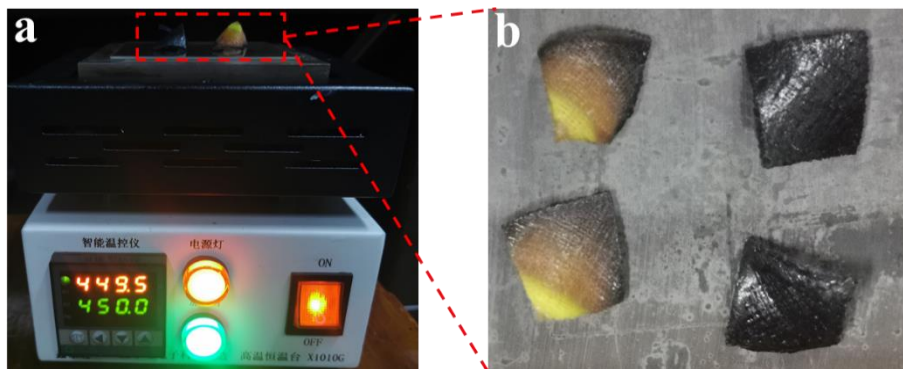
Fig. S18. a) The photograph of the heated platform at work. b) The photograph of 3D-printed PAs after heating to 450 °C.
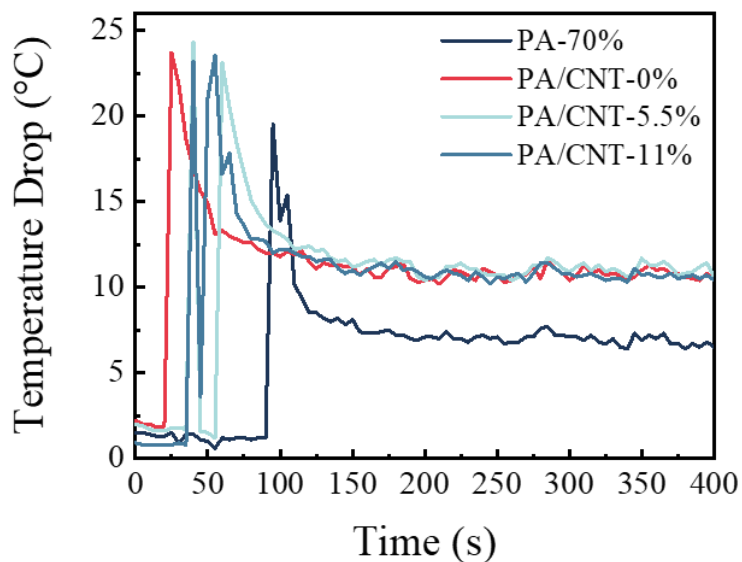
Fig. S19. The temperature drops of 3D-printed PAs at 50 °C heating table. Note that, the various curve initial times are a result of the sample being placed on the same heating table one by one.
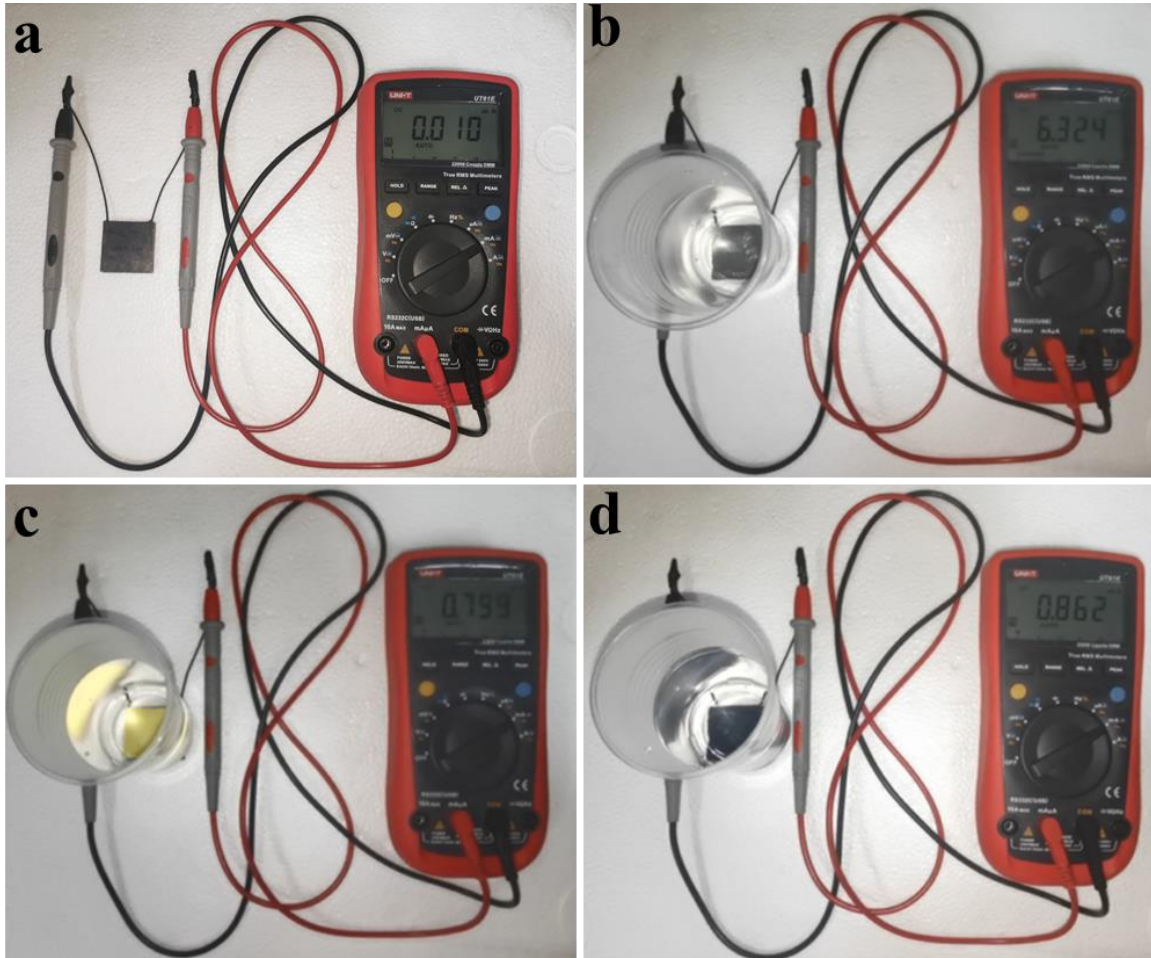
Fig. S20. A thermal insulation demonstration of samples via a temperature difference generation sheet: the experiment setup a), a cup of hot water is placed directly on the hot end of the temperature difference generation sheet b), a cup of hot water is isolated by PA/CNT-0% with ~4 mm of thickness c), and a cup of hot water is isolated by PA/CNT-11% with ~4 mm of thickness d), respectively.
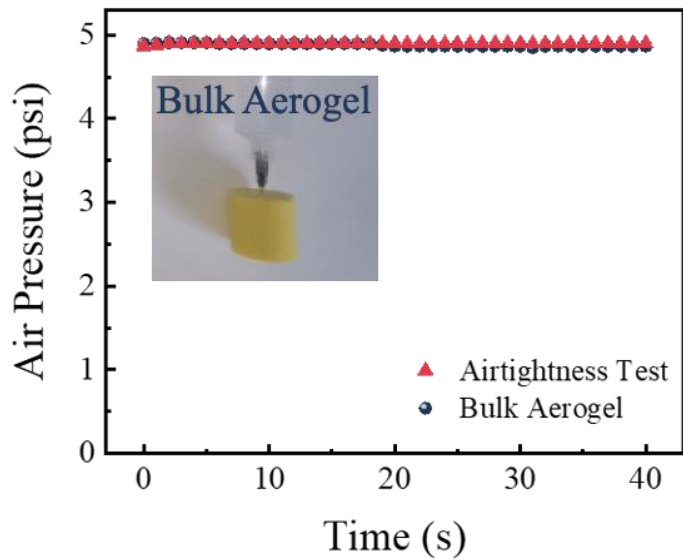
Fig. S21. Airtightness test of experiment setup, and air permeability test of a conventional bulk polyimide aerogel (insert).

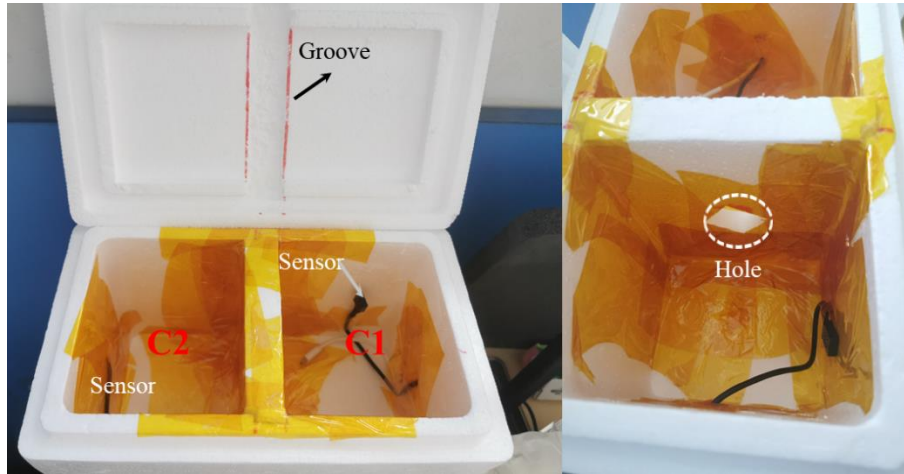**Fig. S22.** A designed simplistic experiment setup of ammonia adsorption tests.

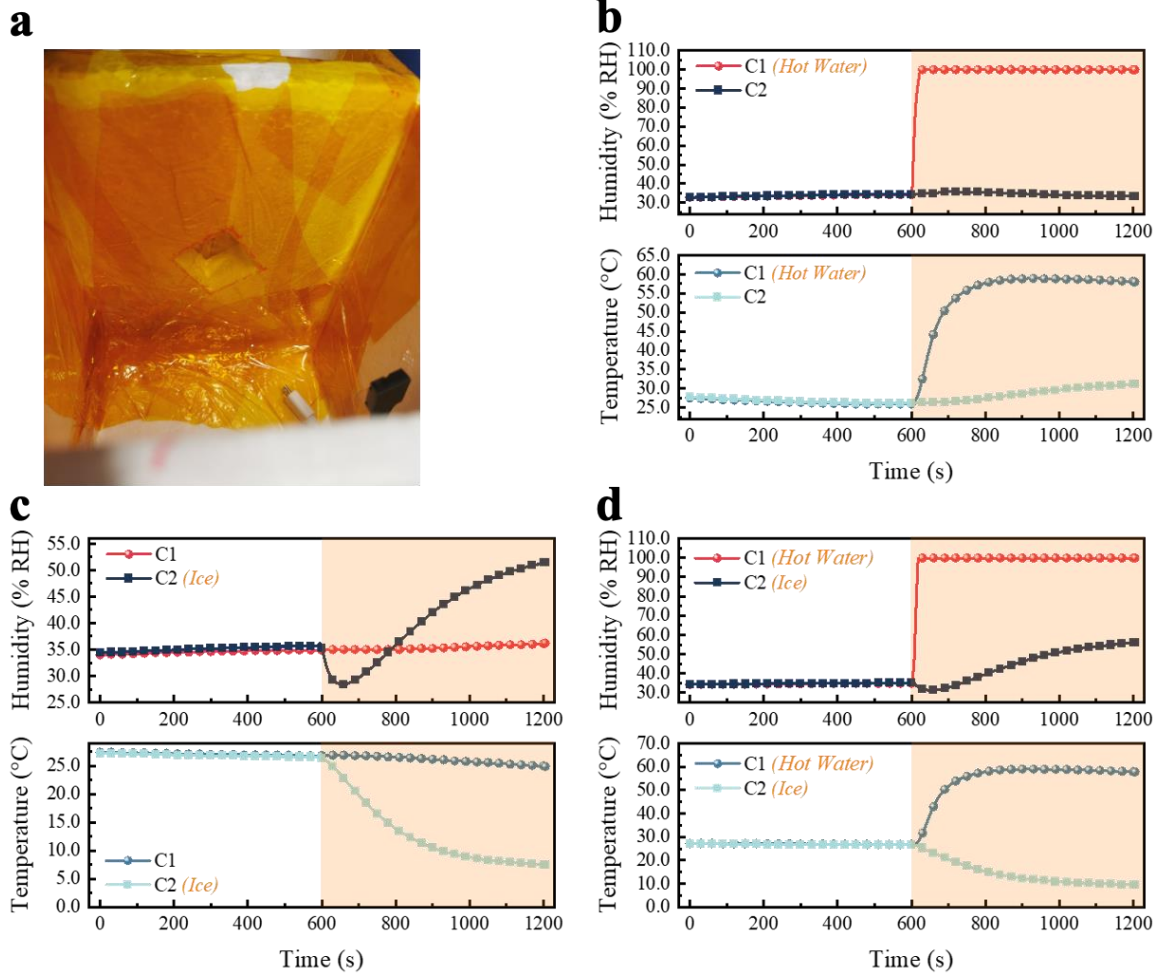**Fig. S23.** The thermal and/or humidity regulation experiment setup.

Fig. S24. Verification of the experiment setup sealing and independence. a) The tightly taped sample hole on the middle foam partition. b-d) Three added conditions, including b) hot water (C1), c) ice pack (C2), and d) a combination of hot water (C1) and ice pack (C2).
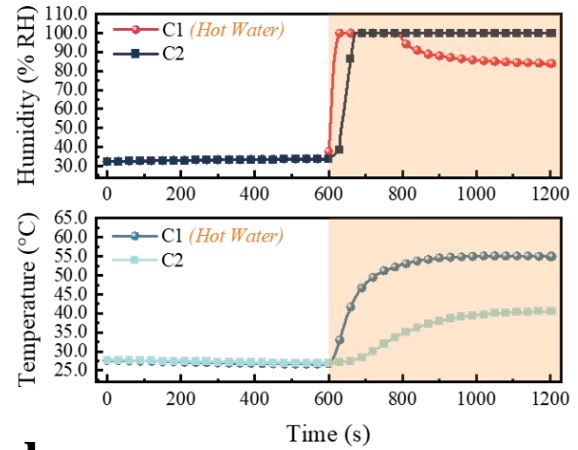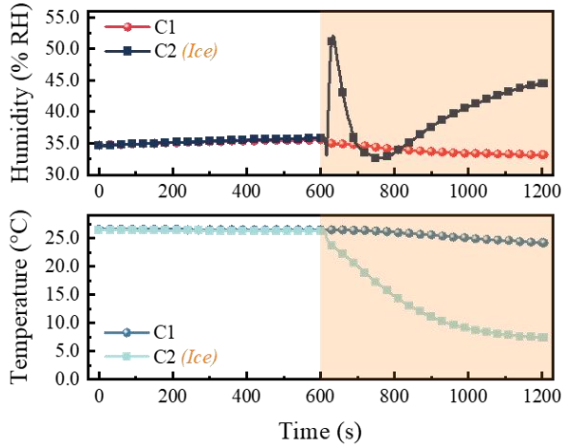
Fig. S25. The thermal and/or humidity regulation experiment: the opened sample hole as control. a) The opened sample hole on the middle foam partition. b-d) Three added conditions, including b) hot water (C1), c) ice pack (C2), and d) a combination of hot water (C1) and ice pack (C2).
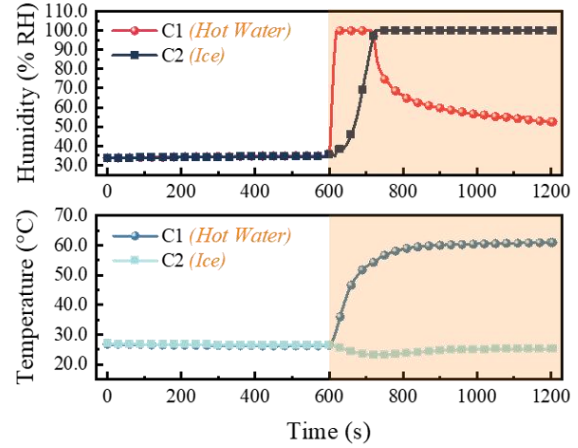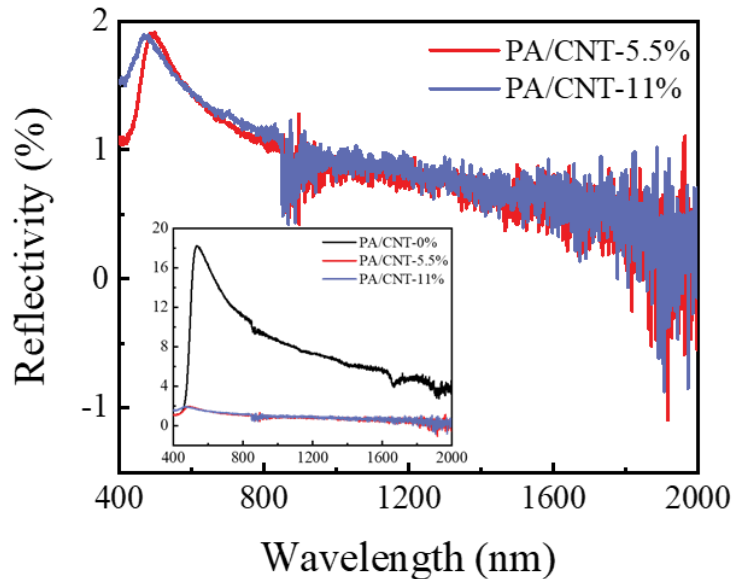
Fig. S26. The reflectivity of 3D-printed quadrate PAs: PA/CNT-0%, PA/CNT-5.5%, PA/CNT-11%.
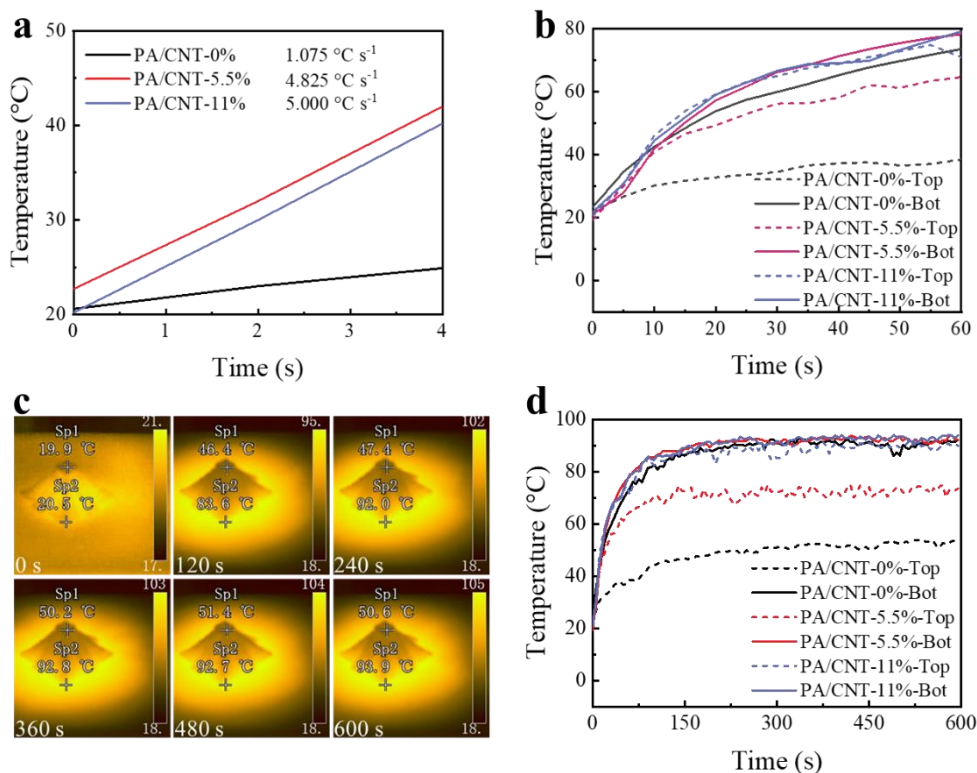

Fig. S27. a) The photothermal response rate of 3D-printed quadrate-shaped PAs for the first 4 s. b) The photothermal response curve of 3D-printed tower-shaped PAs (top and bottom surfaces) for the first 60 s. c) The infrared thermal images of 3D-printed tower-shaped PA (PA/CNT-0%)

under one-sun illumination for 600 s. d) Temperature changes (top and bottom surfaces) of 3D-printed tower-shaped PAs under one-sun illumination for 600 s.
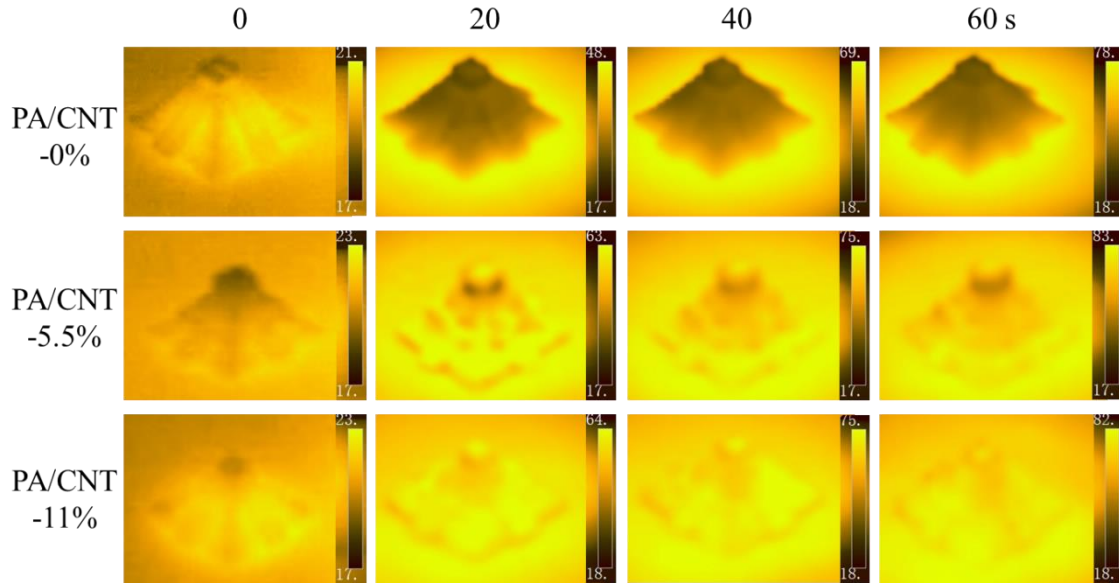

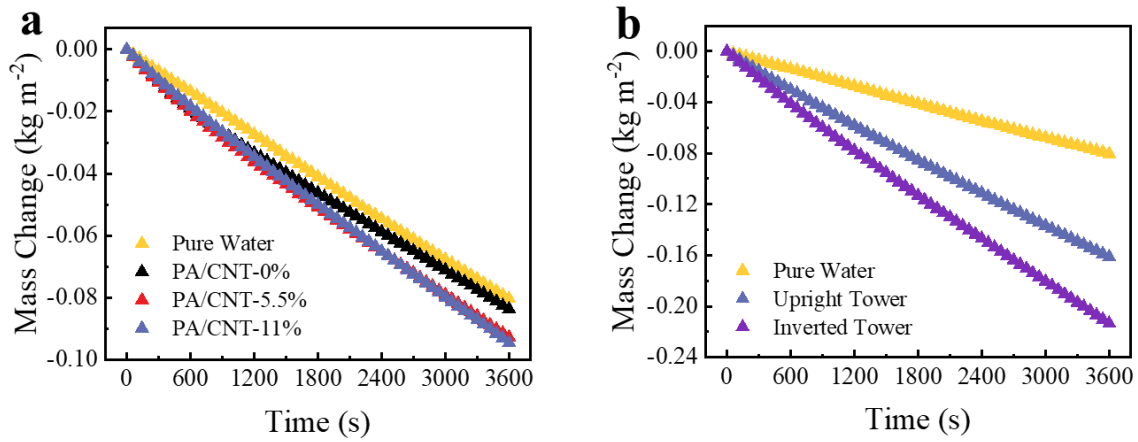**Fig. S28.** The infrared thermal images of 3D-printed tower-shaped PAs.

Fig. S29. Mass changes of water caused by a) 3D-printed quadrate-shaped PA evaporators and b) 3D-printed tower-shaped PA evaporators over time in the darkness.

3. Supplementary Tables

Table S1. The related properties of 3D-printed PAs via DIW.

Ref	Sample Label	S_{BET} (m² g⁻¹)	ρ (mg cm⁻³)	λ (mW m⁻¹ K⁻¹)	ε (%)	T_5 (°C)	Notes
[32]	PA	31	~100	/	/	~200	Instantaneously triggered sol-gel transition in a water reservoir, poor adhesion between adjoining layers
[33]	PI/CNC	/	/	89.39	~25	~300	Heterogeneous rheological modifiers (cellulose nanocrystals), thermal imidization
[34]	PI	/	640	/	~14	~475	Multi-step synthesis strategy, need pore-forming agent and rheological modifier, thermal imidization, oil storage application
[36]	PI	/	/	/	<8	<400	Heterogeneous UV-curable agents, dense structure, thermal imidization
This Work	PA-70%	561.7	66.1±1.4	50.86±0.31	6.99±0.28	~450	Simple and flexible one-step chemical-imidization strategy,
	PA/CNT-0%	561.7	71.6±0.9	39.89±0.16	6.67±0.19	~450	
	PA/CNT-5.5%	553.7	83.3±0.9	45.05±0.22	4.38±0.17	~450	
	PA/CNT-11%	545.1	103.7±1.2	47.51±0.63	4.18±0.08	~450	

Ref	Sample Label	S_{BET} (m² g⁻¹)	ρ (mg cm⁻³)	λ (mW m⁻¹ K⁻¹)	ε (%)	T_5 (°C)	Notes
							multiple functions and expanded applications

S_{BET}, ρ, λ, ε, and T_5 are the specific surface area, density, thermal conductivity, shrinkage, and the temperature corresponding to a 5% decrease in mass of 3D-printed PAs, respectively. "/" indicates "Not measured".

Table S2. The nomenclature and denotation for the acronyms of samples.

Nomenclature	Denotation	Nomenclature	Denotation
PA	Polyimide aerogel	PAA	Polyamide acid
PAs	Polyimide aerogels	PA/CNT	Polyimide aerogel composite
PAAS	polyamide acid ammonium salts		

Table S3. The related parameters of 3D printing by using the PA inks.

PA Inks	Applied Pressure Range (psi or bar)	Actual Printable Interval (min)
PA-C	70-85 or (≈4.83-≈5.86)	<10
PA-D	40-85 or (≈2.76-≈5.86)	~120
PA-E	10-85 or (≈0.69-≈5.86)	/

"/" indicates "Not measured".

Table S4. The gel point and printable interval for the PA/CNT inks.

PA/CNT Inks	Gel Point (h)	Printable Interval (h)
PA/CNT-0%	3.62	2.98
PA/CNT-5.5%	3.05	2.14
PA/CNT-11%	2.88	1.87

Table S5. The detailed parameters of 3D-printed PAs.

3D-Printed PAs	d_1 (mm)	d_2 (mm)	δ (mm)	m (mg)	$\bar{\rho}$ (mg cm^{-3})	ρ_{SD} (mg cm^{-3})	$\bar{\varepsilon}$ (%)	ε_{SD} (%)	$\bar{\lambda}$ (W m^{-1} K^{-1})	λ_{SD} (W m^{-1} K^{-1})
PA-70%	28.91	28.86	3.16	178.6	66.1	1.4	6.99	0.28	0.05086	0.00031
	28.84	29.05	3.23	176.6						
	29.04	28.90	3.25	178.0						
PA/CNT-0%	28.89	29.01	5.86	355.0	71.6	0.9	6.67	0.19	0.03989	0.00016
	28.96	29.01	5.88	349.1						
	28.99	29.03	5.89	356.8						
PA/CNT-5.5%	29.35	29.30	5.13	368.2	83.3	0.9	4.38	0.17	0.04505	0.00022
	29.22	29.41	5.23	370.1						
	29.36	29.37	5.05	366.2						
PA/CNT-11%	29.35	29.38	5.48	492.1	103.7	1.2	4.18	0.08	0.04751	0.00063
	29.28	29.43	5.40	476.5						
	29.44	29.32	5.42	489.4						

d_1, d_2, δ, and m are the length, width, thickness, and mass of 3D-printed PAs, respectively. $\bar{\rho}$, ρ_{SD}, $\bar{\lambda}$, λ_{SD}, $\bar{\varepsilon}$ and ε_{SD} represent the average density, density standard deviation, average thermal conductivity, thermal conductivity standard deviation, average shrinkage, and shrinkage standard deviation of three measurements, respectively.

References

S1   J. Yang, H. Wang, B. Zhou, J. Shen, Z. Zhang and A. Du, *Langmuir,* 2021, **37**, 2129-2139.

S2   G. Shaaban Ibrahim, P. Rizzuto Joseph, A. El-Nemr, L. Bohan, H. Ahmed and H. Tindyebwa, *J. Mater. Civ. Eng.,* 2021, **33**, 04020472.

S3   H. X. Li, H. F. Wen, J. Li, J. C. Huang, D. Wang and B. Z. Tang, *ACS Appl. Mater. Interfaces,* 2020, **12**, 26033-26040.

S4   S. Chaule, J. Hwang, S.-J. Ha, J. Kang, J.-C. Yoon and J.-H. Jang, *Adv. Mater.,* 2021, **33**, 2102649.